

Synthesis and characterization of Y-doped ZnO thin films prepared by spin-coating technique

Abdelhamid Bouaine^{a, b, c}, Hassan Guendouz^a, Guy Schmerber^c, Yasmina Zehouma^a

^aLaboratoire Physique de la Matière Condensée et Nanomatériaux (LPMCN), département de physique, Faculté des Sciences Exactes et Informatique, Université de Jijel, BP 98, OuledAïssa, 18000 Jijel, Algeria.

^bLaboratoire d'Etude des Matériaux (LEM), département de physique, Faculté des Sciences Exactes et Informatique, Université de Jijel, BP 98, OuledAïssa, 18000 Jijel, Algeria.

^cUniversité de Strasbourg, CNRS, Institut de Physique et Chimie des Matériaux de Strasbourg, UMR 7504, 23 rue du Loess, F-67000 Strasbourg, France.

Correspondence Author: Abdelhamid Bouaine, Laboratory Physics of Condensed Matter and Nanomaterials (LPMCN), Department of Physics, Faculty of Exact Sciences and Computer Science, University of Jijel, Algeria.

Received date: 20 May 2019, Accepted date: 20 July 2019, Online date: 28 July 2019

Copyright: © 2019 Abdelhamid Bouaine *et al.*, This is an open-access article distributed under the terms of the Creative Commons Attribution License, which permits unrestricted use, distribution, and reproduction in any medium, provided the original author and source are credited.

Abstract

In this work, we have prepared yttrium (Y) doped ZnO thin films on glass substrates by sol-gel spin-coating technique. Yttrium was incorporated with different concentrations of 2 and 3 at. %. X-ray diffraction analysis shows that all the films are polycrystalline with a hexagonal wurtzite structure and a preferred orientation along the (002) plane. The highest transparency in the visible region was 88%, the largest band gap was 3.23 eV, the lowest electronic disorder was 154.42 meV, and the lowest electrical resistivity was $2.62 \times 10^{-3} \Omega \cdot \text{cm}$. These results were obtained for Y content of 2 at. %.

Keywords: Spin-coating; TCOs; Y doped ZnO; Urbach energy

INTRODUCTION

The most transparent conducting oxide that has been exposed to intensive researches is zinc oxide, given its interest to make progress in numerous nanotechnological fields. ZnO exhibits wide bandgap of 3.37 eV, large exciton binding energy of 60 meV at ambient temperature, excellent transparency, low production cost, non-toxicity, and good stability (Sang et al, 2018; Zhang et al, 2016; Samavati et al, 2017; Li et al, 2015; Shaban et al, 2018; Stehr et al, 2015). The main applications of zinc oxide include solar cells, light-emitting diodes, laser diodes, piezoelectric devices, photosensors, thin-film transistors, auto-heaters, paints, antibacterial agents, biosensors, gas sensors, and photocatalysts (Mudusu et al, 2016; Park et al, 2015; Akhtarianfar et al, 2017; Gupta et al, 2016; Yu et al, 2016; Wu et al, 2016; Rajendran et al, 2016; Kim et al, 2017; Wang et al, 2015).

The synthesis procedure using sol-gel technique is simple and leads to produce homogenous and stoichiometrically controlled ZnO thin films (Ghosh et al., 2017).

ZnO doping with cations, such as aluminum (Al), gallium (Ga), molybdenum (Mo), fluorine (F), niobium (Nb), ytterbium (Yb), have been studied to improve the structural, optical and electrical properties of ZnO thin films. In particular, yttrium incorporation improves the UV emission intensity and enhances photocatalysts efficiency, which promotes the fabrication of the optoelectronic device such as UV detectors and display-screens (Viswanath et al., 2014).

In this work, we aim to obtain Y-doped ZnO thin films on glass substrates with an electrical resistivity of the order of $10^{-3} \Omega \cdot \text{cm}$ and high transparency ($\approx 80\%$) for Y doping concentrations of 2 and 3 at. % using the sol-gel spin-coating technique. The effects of Y doping on the structural, optical, and electrical properties of ZnO nanostructures were investigated in some details.

EXPERIMENTAL PROCEDURES

Y doped zinc oxide thin films with 2 and 3 at. % concentrations were synthesized by sol-gel spin-coating method. As starting materials, zinc acetate dihydrate ($\text{Zn}(\text{CH}_3\text{COO})_2 \cdot 2\text{H}_2\text{O}$), and Yttrium nitrate hexahydrate ($\text{Y}(\text{NO}_3)_3 \cdot 6\text{H}_2\text{O}$) were used. For each case, zinc acetate dihydrate ($\text{Zn}(\text{CH}_3\text{COO})_2 \cdot 2\text{H}_2\text{O}$) as a metal precursor was first dissolved in 5 ml of isopropanol ($(\text{CH}_3)_2\text{CHOH}$) and then it was mixed with the doping precursor which was separately dissolved in 5 ml of ethanol ($\text{CH}_3\text{CH}_2\text{OH}$) with desired

concentration to obtain a total mixture volume of 10 ml. Few drops of mono-ethanolamine (MEA) were used to stabilize the mixtures. Each mixture simultaneously stirred and heated at 60°C for 2 hours on a magnetic agitator hot plate to obtain a transparent and homogenous solution.

These solutions with a molar concentration of 0.2 M were deposited on glass substrates using the spin-coating technique. A little portion of each solution was deposited and rotated on a glass substrate for 30 seconds with a speed of 2200 rpm to give a thin film which was heated for five minutes at 300°C to remove organic residuals such as isopropanol, ethanol and MEA. This operation was repeated ten times to achieve the required thickness and then all thin films were annealed at 500°C during 1 hour for the crystallization.

The structural properties of the films were analyzed in the θ - 2θ configuration using a Bruker D8 Advance diffractometer (40 mA, 40 kV) equipped with a Sol^X detector and using the monochromatic $\text{CuK}_{\alpha 1}$ radiation ($\lambda = 0.154056$ nm). The optical properties of the films were determined using a UV-Vis Perkin-Elmer Lambda 950 spectrophotometer at room temperature. JANDEL four-point probe and Dektak 150 profilometer were used to measure the electrical resistivity and thickness of thin films, respectively.

RESULTS AND DISCUSSION

Structural properties

Figure 1 shows the room-temperature X-ray diffraction pattern of Y doped ZnO films deposited on glass substrates and annealed in air ambient at 500 °C for one h. All the films are polycrystalline with expected hexagonal wurtzite structure, and no additional phases such as Y_2O_3 and In_2O_3 could be detected. The increase in yttrium doping concentration deteriorates further the crystallinity. The preferential orientation was along c-axis perpendicular to the substrate where the (002) peak positions for 2 and 3 at.% concentrations were shifted to be 34.46 and 34.40°, respectively as compared to the standard diffraction angle (2θ) which is 34.45° (JCPDS Card No. 36-1451).

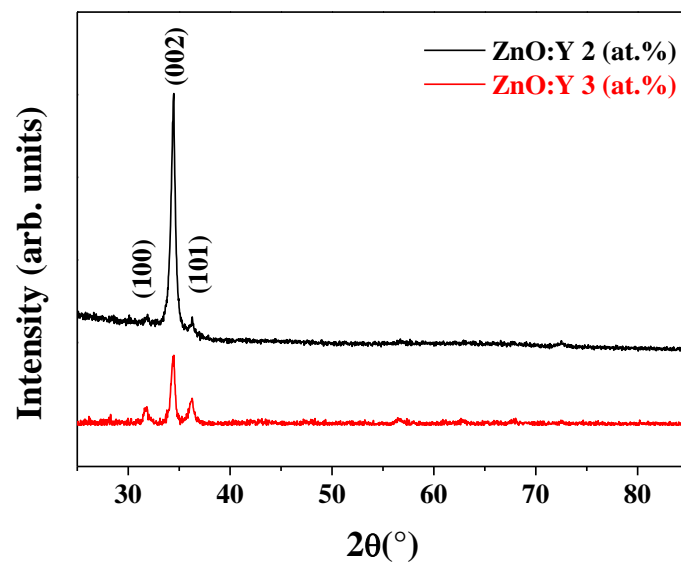


Fig. 1: XRD patterns of Y doped ZnO thin films.

The lattice parameter (c) is calculated using the following formula (Farhat et al, 2015).

$$\frac{1}{d_{(hkl)}^2} = \frac{4}{3} \left(\frac{h^2 + hk + k^2}{a^2} \right) + \frac{l^2}{c^2}$$

Where the interplanar distance $d_{(hkl)}$ is calculated using Bragg's law (Lupan et al, 2010).

$$n\lambda = 2 d_{(hkl)} \sin \theta$$

Y incorporation with 2 at. % concentration reduced the lattice parameter to be found 5.201 Å in compared with a standard value which is 5.205 Å (JCPDS Card No. 36-1451) whereas Y incorporation with 3 at.% concentration increased the lattice parameter to be found 5.210 Å which is higher than the standard value. Yttrium substitution in zinc sites produces lattice parameter extension since Y^{3+} ionic radius (0.89Å) is higher than Zn^{2+} one (0.74 Å) reflecting the lattice parameter increase (Yu et al., 2007).

For ZnO: Y (2 at. %), yttrium segregated in grain boundaries caused a dominant compressive strain over the extensive strain originated from Y^{3+} ions substituted in Zn^{2+} sites explaining the lattice parameter decrease. It is possible that low Y quantity

segregated in grain boundaries produces dominant compressive strain in the case of small grain size. In revenge, ZnO: Y (3 at. %) was exposed to an extensive dominant strain leading to lattice parameter increase.

The grain size (D) of yttrium doped zinc oxide thin films is calculated using the Scherrer formula (Pan et al., 2013).

$$D = \frac{k \lambda}{\beta \cos \theta}$$

Where k is constant ($k = 0.9$), λ is the X-ray radiation wavelength, β is the full width at half maximum (FWHM) for (hkl) plane, and θ is the diffraction angle.

Increasing Y doping concentration from 2 to 3 at. % increased the grain size (along c-axis) from 31.56 to 32.25 nm. Nevertheless, the diffraction intensity of ZnO: Y (3 at. %) remains less than that of ZnO:Y (2 at.%) since the number of crystallites doped with Y 3 at.% concentration is noticeably lower than the number of crystallites doped with Y 2 at.% concentration.

Optical properties

The transmittance spectra of Y doped ZnO thin films are given in the [200-900] nm wavelength region as shown in figure 2. After doping with 2 and 3 at. % of Y, high transmittance was observed to be 88 and 84%, respectively. The optical band gap of Yttrium doped zinc oxide thin films is estimated using Tauc's plot (Senadim et al., 2006).

$$\alpha h\nu = A(h\nu - E_g)^{1/2}$$

Where α , $h\nu$, A , and E_g are the absorption coefficient, photon energy, constant, and optical bandgap, respectively.

According to figure 3, the optical band gap was found to be 3.23 and 3.22 eV for ZnO: Y (2 at. %) and ZnO: Y (3 at.%), respectively. This diminution with increasing Y content is due to the existence of localized defect states into the forbidden band (Bouaine et al., 2018).

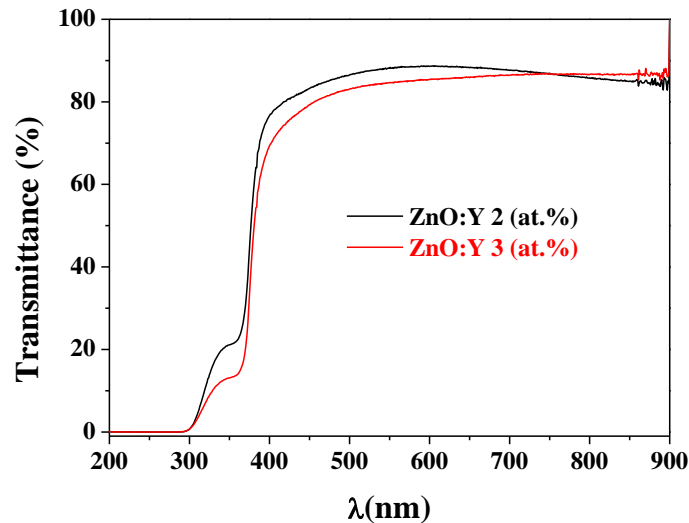


Fig. 2: Transmittance spectra of Y doped ZnO thin films.

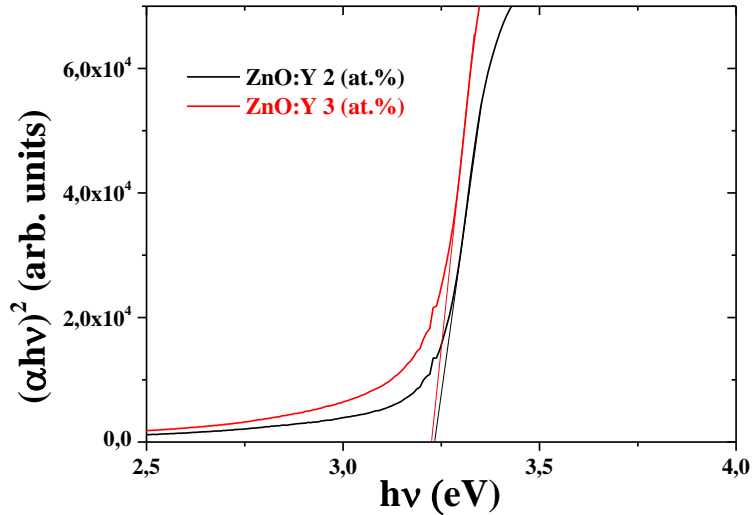


Fig. 3: Optical band gap of Y doped ZnO thin films.

Urbach energy which determines the disorder is defined as the width of localized states tail into the forbidden band (Guendouz *et al.*, 2018). The following equation is used to calculate Urbach energy (Bai *et al.*, 2012).

$$\alpha = \alpha_0 \exp\left(\frac{h\nu}{E_U}\right)$$

Where α_0 is constant.

The Urbach energy E_U is the slope inverse of the linear part of the curve $\ln(\alpha)$ against $h\nu$.

Yttrium incorporation with 2 to 3 at. % led to obtaining Urbach energy of 154.42 and 178.49 meV, respectively (Fig. 4). The increase in Y content creates more disorder.

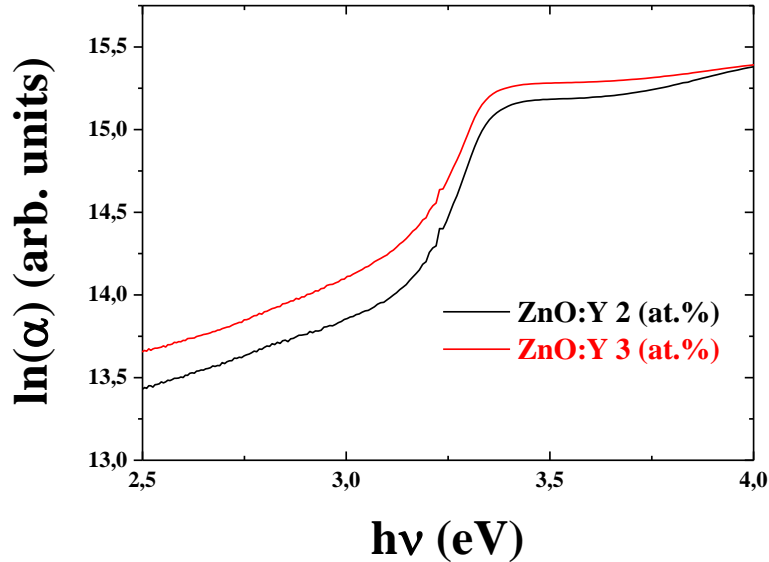


Fig. 4: Urbach energy of Y doped ZnO thin films.

Electrical properties

The electrical resistivity values of ZnO:Y (2 at.%) and ZnO:Y (3 at.%) were 2.62×10^{-3} and $3.51 \times 10^{-3} \Omega \cdot \text{cm}$, respectively (Fig. 5). The yttrium introduced in ZnO thin films is divided into two portions; Y^{3+} ions that substitute Zn^{2+} sites in the grains act as donor dopants and contribute to reducing the resistivity, Y atoms segregated in grain boundaries and interstitial Y act as passive dopants and have no improvement on resistivity (Yu *et al.*, 2007). ZnO thin film doped with Y 2 at. % concentration contains a high amount of grains. The quantity of Y^{3+} ions substituting Zn^{2+} sites in these grains is higher than the quantity of Y segregated in grain boundaries and interstitial Y, which justifies the low resistivity obtained for Y 2 at.% concentration. ZnO thin film doped with Y 3 at. % concentration contains a low amount of relatively large grains which are located in remarkably deformed ZnO structure. Hence, the quantity of Y^{3+} ions substituting Zn^{2+} sites in these grains is insufficient to reduce the resistivity. Furthermore, the remained quantity of Y atoms which are distributed in highly deformed ZnO has a weak contribution to resistivity lowering.

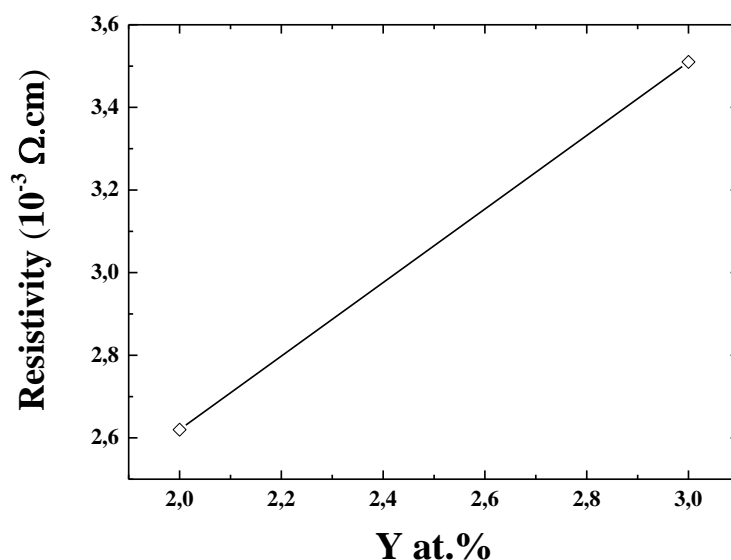


Fig. 5: Resistivity variation of Y doped ZnO thin films.

CONCLUSION

This work shows the possibility of synthesizing yttrium doped zinc oxide thin films onto glass substrates by using the sol-gel spin-coating technique. The influences of Y doping concentration on the structural, optical, and electrical properties of ZnO thin films have been investigated by X-ray diffraction (XRD), UV-visible spectrophotometer, and Four-Point probe techniques. The films of Y doped ZnO exhibit high transmittance in the visible range, large bandgap, and low electrical resistivity in the order of $10^{-3} \Omega \cdot \text{cm}$. These properties make zinc oxide the most required semiconductor in many industrial applications such as solar cells, light-emitting diodes LEDs, photodetectors, and integrated circuits.

ACKNOWLEDGEMENTS

This work carried out at the Laboratory (LPMCN-Algeria), the Institute (IPCMS-France), and Jijel University (project# B00L02UN180120180002) was financed by the Ministry of Higher Education and the Scientific Research (Algeria).

REFERENCES

- Akhtarianfar, S. F., A. Khayatian, R. Shakernejad, M. Almasi-kashi, S. W. Hong, 2017. Improved sensitivity of UV sensors in hierarchically structured arrays of network-loaded ZnO nanorods via optimization techniques. *Royal Society of Chemistry Advances*, 7:32316–32326. doi:10.1039/c7ra04773h.
- Bai, W., W. F. Xu, J. Wu, J. Y. Zhu, G. Chen, J. Yang, T. Lin, X. J. Meng, X.D. Tang, J. H. Chu, 2012. Investigations on electrical, magnetic and optical behaviors of five-layered aurivillius $\text{Bi}_6\text{Ti}_3\text{Fe}_2\text{O}_{18}$ polycrystalline films. *Thin Solid Films*, 525:195–199. doi:10.1016/j.tsf.2012.10.058.
- Bouaine, A., A. Bourebia, H. Guendouz, Z. Riane, 2018. Synthesis and characterization of In doped ZnO thin film as efficient transparent conducting oxide candidate. *Optik*, 166:317–322. doi:10.1016/j.ijleo.2018.04.017.
- Farhat, O.F., M.M. Halim, M.J. Abdullah, M.K.M. Ali, N.K. Allam, 2015. Morphological and structural characterization of single-crystal ZnO nanorod arrays on flexible and non-flexible substrates. *Beilstein Journal of Nanotechnology*, 6:720–725. doi:10.3762/bjnano.6.73.
- Ghosh, S., D. Basak, 2017. A simple process step for tuning the optical emission and ultraviolet photosensing properties of sol-gel ZnO film. *Royal Society of Chemistry Advances*, 7:694–703. doi:10.1039/c6ra25921a.
- Guendouz, H., A. Bouaine, N. Brihi, 2018. Biphasic effect on structural, optical, and electrical properties of Al-Sn codoped ZnO thin films deposited by sol-gel spin-coating technique. *Optik*, 158:1342–1348. doi:10.1016/j.ijleo.2018.01.025.
- Gupta, K., J. Lin, R. Wang, C. Liu, 2016. Porosity-induced full-range visible-light photodetection via ultrahigh broadband antireflection in ZnO nanowires. *NPG Asia Materials*, 8:e314. doi:10.1038/am.2016.147.
- Kim, D., W. Kim, S. Jeon, 2017. Highly efficient UV-sensing properties of Sb-doped ZnO nanorod arrays synthesized by a facile single-step hydrothermal reaction. *Royal Society of Chemistry Advances*, 7:40539–40548. doi:10.1039/c7ra07157d.
- Li, S., Z. Sun, R. Li, M. Dong, L. Zhang, W. Qi, X. Zhang, H. Wang, 2015. ZnO nanocomposites modified by hydrophobic and hydrophilic silanes with dramatically enhanced tunable fluorescence and aqueous ultrastability toward biological imaging applications. *Scientific Reports*, 5:8475. doi:10.1038/srep08475.
- Lupan, O., T. Pauporté, L. Chow, B. Viana, F. Pellé, L.K. Ono, B. R. Cuenya, H. Heinrich, 2010. Effects of annealing on properties of ZnO thin films prepared by electrochemical deposition in chloride medium. *Applied Surface Science*, 256:1895–1907. doi:10.1016/j.apsusc.2009.10.032.

- Mudusu, D., K. R. Nandanapalli, S. R. Dugasani, 2016. Zinc oxide nanorods shielded with an ultrathin nickel layer: tailoring of physical properties, *Scientific Reports*, 6:28561. doi:10.1038/srep28561.
- Pan, Z., X. Tian, G. Hu, C. Xiao, Z. Wei, S. Wu, Z. Li, J. Deng, 2013. Investigation of optical and electronic properties in Al-Sn co-doped ZnO thin films. *Materials Science in Semiconductor Processing*, 16:587–592. doi:10.1016/j.mssp.2012.06.020.
- Park, G. C., S. M. Hwang, S. M. Lee, J. H. Choi, K. M. Song, H. Y. Kim, H. Kim, S. Eum, S. Jung, J. H. Lim, 2015. Hydrothermally grown In-doped ZnO nanorods on p-GaN films for Color-tunable heterojunction light-emitting-diodes. *Scientific Reports*, 5:10410. doi: 10.1038/srep10410.
- Rajendran, S., M. M. Khan, F. Gracia, J. Qin, 2016. Ce³⁺-ion-induced visible-light photocatalytic degradation and electrochemical activity of ZnO/CeO₂ nanocomposite. *Scientific Reports*, 6:31641. doi: 10.1038/srep31641.
- Samavati, A., Z. Samavati, A.F. Ismail, M.H.D. Othman, 2017. Structural, optical and electrical evolution of Al and power density, *Royal Society of Chemistry Advances*, 7:35858–35868. doi:10.1039/c7ra04963c.
- Sang, D., Q. Wang, Q. Wang, W. Wang, B. Zhang, Q. Fan, 2018. Improved electrical transport properties of an n-ZnO nanowire/p-diamond heterojunction. *Royal Society of Chemistry Advances*, 8:28804–28809. doi:10.1039/c8ra03546f.
- Senadim, E., H. Kavak, R. Esen, 2006. The effect of annealing on structural and optical properties of ZnO thin films grown by pulsed filtered cathodic vacuum arc deposition. *Journal of Physics: Condensed Matter*, 18:6391–6400. doi:10.1088/0953-8984/18/27/021.
- Shaban, M., F. Mohamed, S. Abdallah, 2018. Production and characterization of superhydrophobic and antibacterial coated fabrics utilizing ZnO nanocatalyst. *Scientific Reports*, 8:3925. doi:10.1038/s41598-018-22324-7.
- Stehr, J. E., W. M. Chen, N. K. Reddy, C. W. Tu, I. A. Buyanova, 2015. Efficient nitrogen incorporation in ZnO nanowires. *Scientific Reports*, 5:13406. doi: 10.1038/srep13406.
- Viswanath, R., H. S. B. Naik, Y. K. G. Somalanaik, P. K. P. Neelanjaneallu, K. N. Harish, M. C. Prabhakara, 2014. Studies on characterization, optical absorption, and photoluminescence of yttrium doped ZnS nanoparticles. *Journal of Nanotechnology*, 2014:924797–924804. doi:10.1155/2014/924797.
- Wang, M., F. Ren, J. Zhou, G. Cai, L. Cai, Y. Hu, 2015. N doping to ZnO nanorods for photoelectrochemical water splitting under visible light: engineered impurity distribution and terraced band structure. *Scientific Reports*, 5:12925. doi: 10.1038/srep12925.
- Wu, X., J. Lee, V. Varshney, J.L. Wohlwend, A.K. Roy, 2016. Thermal conductivity of wurtzite zinc-oxide from first-principles lattice dynamics - a comparative study with gallium nitride. *Scientific Reports*, 6:22504. doi: 10.1038/srep22504.
- Yu, Q., W. Fu, C. Yu, H. Yang, R. Wei, Y. Sui, S. Liu, Z. Liu, G. Zou, 2007. Structural, electrical and optical properties of yttrium-doped ZnO thin films prepared by sol – gel method. *Journal of Physics D: Applied Physics*, 40:5592–5597. doi:10.1088/0022-3727/40/18/014.
- Yu, S., L. Li, X. Lyu, W. Zhang, 2016. Preparation and investigation of nano-thick FTO/Ag/FTO multilayer transparent electrodes with high figure of merit. *Scientific Reports*, 6:20399. doi: 10.1038/srep20399.
- Zhang, Y., N. Lin, Y. Li, X. Wang, H. Wang, J. Kang, 2016. The isotype ZnO/SiC heterojunction prepared by molecular beam epitaxy – a chemical inert interface with significant band discontinuities. *Scientific Reports*, 6:23106. doi: 10.1038/srep23106.